

Article

Ferrocene-functionalized zirconium-oxo clusters for achieving high-performance thermocatalytic redox reactions

Su-Juan Yao, Jiao-Min Lin, Long-Zhang Dong, Ying-Lin Li, Ning Li, Jiang Liu, Ya-Qian Lan

PII: S2095-9273(24)00134-8  
DOI: <https://doi.org/10.1016/j.scib.2024.02.032>  
Reference: SCIB 2615

To appear in: *Science Bulletin*

Received Date: 17 November 2023  
Revised Date: 7 January 2024  
Accepted Date: 19 February 2024



Please cite this article as: S-J. Yao, J-M. Lin, L-Z. Dong, Y-L. Li, N. Li, J. Liu, Y-Q. Lan, Ferrocene-functionalized zirconium-oxo clusters for achieving high-performance thermocatalytic redox reactions, *Science Bulletin* (2024), doi: <https://doi.org/10.1016/j.scib.2024.02.032>

This is a PDF file of an article that has undergone enhancements after acceptance, such as the addition of a cover page and metadata, and formatting for readability, but it is not yet the definitive version of record. This version will undergo additional copyediting, typesetting and review before it is published in its final form, but we are providing this version to give early visibility of the article. Please note that, during the production process, errors may be discovered which could affect the content, and all legal disclaimers that apply to the journal pertain.

## Article

Received 17 November 2023

Received in revised form 7 January 2024

Accepted 19 February 2024

**Ferrocene-functionalized zirconium-oxo clusters for achieving high-performance thermocatalytic redox reactions**Su-Juan Yao<sup>1</sup>, Jiao-Min Lin<sup>1</sup>, Long-Zhang Dong, Ying-Lin Li, Ning Li, Jiang Liu\*, Ya-Qian Lan\*

School of Chemistry, South China Normal University, Guangzhou 510006, China

\*Corresponding Authors: [liuj0828@m.scnu.edu.cn](mailto:liuj0828@m.scnu.edu.cn) (J. Liu); [yqlan@m.scnu.edu.cn](mailto:yqlan@m.scnu.edu.cn) (Y.-Q. Lan)<sup>1</sup> These authors contributed equally to this work.

**Abstract:** The Zr(IV) ions are easily hydrolyzed to form oxides, which severely limits the discovery of new structures and applications of Zr-based compounds. In this work, three ferrocene (Fc)-functionalized Zr-oxo clusters (ZrOCs), **Zr<sub>9</sub>Fc<sub>6</sub>**, **Zr<sub>10</sub>Fc<sub>6</sub>** and **Zr<sub>12</sub>Fc<sub>8</sub>** were synthesized through inhibiting the hydrolysis of Zr(IV) ions, which show increased nuclearity and regular structural variation. More importantly, these Fc-functionalized ZrOCs were used as heterogeneous catalysts for the transfer hydrogenation of levulinic acid (LA) and phenol oxidation reactions for the first time, and displayed outstanding catalytic activity. In particular, **Zr<sub>12</sub>Fc<sub>8</sub>** with the largest number of Zr active sites and Fc groups can achieve >95% yield for LA-to- $\gamma$ -valerolactone within 4 h (130 °C) and >98% yield for 2,3,6-trimethylphenol-to-2,3,5-trimethyl-p-benzoquinone within 30 min (80 °C), showing the best catalytic performance. Catalytic characterization combined with theory calculations reveal that in the Fc-functionalized ZrOCs, the Zr active sites could serve as substrate adsorption sites, while the Fc groups could act as hydrogen transfer reagent or Fenton reagent, and thus achieve effectively intramolecular metal-ligand synergistic catalysis. This work develops functionalized ZrOCs as catalysts for thermal-triggered redox reactions.

**Keywords:** Zirconium-oxo cluster, Metal-ligand synergistic thermalcatalysis, Crystalline coordination compound, Hydrogen transfer, Fenton reagent

**1. Introduction**

Zirconium dioxide (ZrO<sub>2</sub>) possesses excellent catalytic activity in some specific catalytic reactions, such as the Fischer-Tropsch process and carbon dioxide hydrogenation, due to its redox properties, Lewis acid/base properties, and ability to produce oxygen vacancies easily [1–4]. However, the structural changes of ZrO<sub>2</sub> are limited to tetragonal, monoclinic and cubic structures, which hinder the expansion of catalytic reactions [5]. Considering the high coordination number and strong Lewis acidity of Zr(IV) ion, the assembly of Zr-based coordination compounds is considered as an effective strategy to enrich the structural types of ZrO<sub>2</sub> [6,7]. For instance, Zr(IV) ions combined with different oxygen-containing ligands can generate distinct Zr-based compounds [8,9]. However, the number of reported structures of Zr-based compounds is still limited, as Zr(IV) ions are readily hydrolyzed to form ZrO<sub>2</sub>. Crystalline Zr-based compounds, primarily Zr-oxo cluster (ZrOCs)-based metal-organic frameworks (Zr-MOFs, in which [Zr<sub>6</sub>O<sub>8</sub>] cluster is the most common secondary building unit) [10–14], have further expanded the applications of Zr-based compounds in catalytic reactions such as olefin polymerization, hydrogenation, borohydride reduction, and hydrogen amination by effectively combining the dual advantages of ZrOCs and functional ligand [15–18]. Nonetheless, considering that metal ions

are often used as catalytic active sites, the low nuclearity of ZrOCs in Zr-MOFs limits their overall catalytic activity. Additionally, as nuclearity increases, the crystallinity of the Zr-MOFs becomes more challenging [19,20].

Reducing the dimensionality of Zr-MOFs to construct Zr-based coordination compounds has been identified as a potential solution to address the aforementioned issues. For instance, synthesizing ZrOCs can retain the superiority of Zr-oxo core and functional ligand equally, while also allowing the number of metal active sites to increase with increased nuclearity, thereby enhancing catalytic performance [21–24]. Furthermore, compared to Zr-MOFs, ZrOCs have the advantage of exhibiting either homogeneous or heterogeneous catalysis by regulating their solid-state solubility [25,26]. This feature is particularly beneficial for their broad application in catalytic reactions, resulting in improved specific reactivity [16,17,22]. Additionally, the selection of functional ligands is crucial in expanding the catalytic applications of ZrOCs. Considering the structural characteristics of the ligand and possible synergistic metal-ligand catalysis, more types of catalytic reactions could potentially be discovered and achieved through functionalized ZrOCs catalysts. Nevertheless, the use of ligand engineering to modulate the catalytic application and reactivity of ZrOCs is still very rare.

Based on the above considerations, we designed and constructed three nuclearity-increased ferrocene (Fc)-functionalized ZrOCs, **Zr<sub>9</sub>Fc<sub>6</sub>** ( $\text{Zr}_9(\mu_4\text{-O})_3(\mu_3\text{-O})_5(\mu_2\text{-OEt})_6(\text{Fc})_6(\text{OEt})_3(\text{O}^i\text{Pr})_6$ ), **Zr<sub>10</sub>Fc<sub>6</sub>** ( $\text{Zr}_{10}(\mu_4\text{-O})_4(\mu_3\text{-O})_4(\mu_2\text{-OEt})_7(\text{Fc})_6(\text{OEt})_{10}$ ), and **Zr<sub>12</sub>Fc<sub>8</sub>** ( $\text{Zr}_{12}(\mu_4\text{-O})_4(\mu_3\text{-O})_{10}(\mu_2\text{-O}^i\text{Pr})_6(\text{Fc})_8(\text{O}^i\text{Pr})_8$ ). It is well-known that Fc group possesses superior electron-donating ability, redox reversibility and rapid charge transfer due to its sandwich structure with two negatively charged cyclopentadienyl rings [27–32]. Interestingly, these ZrOCs also showed similar characters and significant improvement in charge separation and transfer abilities after being modified by Fc groups. Therefore, they were treated as reductive catalysts for the catalytic conversion of levulinic acid (LA), in which electron-donating Fc groups promoted solvent molecule deprotonation and then synergized with Zr active sites to efficiently accomplish the high-efficient catalytic transfer hydrogenation reaction (Scheme 1a) [33–35]. All three ZrOCs demonstrated high catalytic activities with LA conversion approaching 100%, and they showed that the more Fc groups coordinated on the ZrOCs, the higher of the catalytic activity ( $\gamma$ -valerolactone ( $\gamma$ -GVL) yield: **Zr<sub>12</sub>Fc<sub>8</sub>** > **Zr<sub>10</sub>Fc<sub>6</sub>** > **Zr<sub>9</sub>Fc<sub>6</sub>**). Furthermore, these Fc-functionalized ZrOCs can also serve as catalysts for phenol oxidation, in which Fc groups preferentially acted as Fenton reagent to generate oxygen-containing radicals and then synergized with active peroxozirconate to oxidize the adsorbed 2,3,6-trimethylphenol (TMP) molecule to 2,3,5-trimethyl-pbenzoquinone (TMBQ) efficiently (Scheme 1b) [36,37]. Notably, the increase in Fc groups and active Zr sites in ZrOCs further enhances the catalytic performance. As result, **Zr<sub>12</sub>Fc<sub>8</sub>** achieved the highest catalytic performance with the TMBQ yield of 98.8% within 30 min. This work demonstrates the great potential of ligand engineering strategy in regulating the structural and functional characteristics of ZrOCs, and develops for the first time the application of ZrOCs in transfer hydrogenation of LA-to- $\gamma$ -GVL and phenol oxidation reactions.

**Scheme 1.** (Color online) Illustration of the metal-ligand synergistic catalysis in the ferrocene (Fc)-functionalized Zr-oxo clusters for the (a) transfer hydrogenation of levulinic acid (LA) reaction and (b) 2,3,6-trimethylphenol (TMP) oxidation reaction.

## 2. Materials and methods

The preparation of the samples as well as the testing of the properties is described in detail in Supplementary materials, Experimental Procedures (online). All chemical reagents and solvents used for the synthesis were commercially available and without further purification. We determined the exact structure of the crystals using single-crystal X-ray diffractometer. The products were analyzed by gas chromatography-mass spectrometer (GC-MS).

## 3. Results and discussion

**Zr<sub>9</sub>Fc<sub>6</sub>**, **Zr<sub>10</sub>Fc<sub>6</sub>** and **Zr<sub>12</sub>Fc<sub>8</sub>** were synthesized via solvothermal reaction of metal-alcohol salts and carboxylic acid ligands in mixture/pure alcoholic solvents (Tables S1–S4 online). The use of carboxylic acid ligands and alcoholic solvents are crucial for this reaction since they can coordinate with the Zr(IV) ions, and thus effectively inhibit the hydrolysis of Zr(IV) ions to form ZrO<sub>2</sub> [38]. In addition, the alcoholic solvents may act as terminal coordinated molecules, which make it more easily to create potential opening Zr active sites on the resulting ZrOCs.

Single crystal X-ray diffraction analysis reveals that **Zr<sub>9</sub>Fc<sub>6</sub>**, **Zr<sub>10</sub>Fc<sub>6</sub>** and **Zr<sub>12</sub>Fc<sub>8</sub>** are nine-nuclear, ten-nuclear and twelve-nuclear ZrOCs (Fig. 1a), respectively. **Zr<sub>9</sub>Fc<sub>6</sub>** crystallizes in a trigonal system with the space group *P*-3. The whole molecule of **Zr<sub>9</sub>Fc<sub>6</sub>** consists of a nine-nuclear Zr-oxo core, six Fc ligands, six  $\mu_2$ -OEt and six terminal coordinated O'Pr and three OEt groups (Fig. 1b, c and Fig. S3 online). The nine-nuclear Zr-oxo core is built up by a classic octahedral Zr<sub>6</sub>-oxo core and three Zr-oxo units as caps, featuring a tri-capped octahedron (Fig. S2 online). The Zr ion in the octahedral Zr<sub>6</sub>-oxo core is coordinated by seven O atoms, while the capped Zr ion is coordinated by six O atoms. These Zr ions are connected together by the  $\mu_4$ -O,  $\mu_3$ -O and  $\mu_2$ -OEt to form the nine-nuclear Zr-oxo core. The outer coordination space of this nine-nuclear Zr-oxo core is surrounded by six Fc ligands, six  $\mu_2$ -OEt and nine terminal coordinated O'Pr and OEt groups (Fig. S1 online). Noted that these terminal coordinated O'Pr and OEt groups may easily leave after protonated, which make the Zr atoms can become potential catalytic active sites.

**Fig. 1.** (Color online) Molecular structures of **Zr<sub>9</sub>Fc<sub>6</sub>**, **Zr<sub>10</sub>Fc<sub>6</sub>** and **Zr<sub>12</sub>Fc<sub>8</sub>**. (a) The structures of three Zr-oxo cores, Zr<sub>9</sub>, Zr<sub>10</sub> and Zr<sub>12</sub>, which are extended from the classic Zr<sub>6</sub>O<sub>8</sub> octahedral core. (b) The structures of Zr<sub>9</sub>, Zr<sub>10</sub> and Zr<sub>12</sub> cores after decorated with different numbers of functional Fc groups. (c) The entire structures of **Zr<sub>9</sub>Fc<sub>6</sub>**, **Zr<sub>10</sub>Fc<sub>6</sub>** and **Zr<sub>12</sub>Fc<sub>8</sub>**. All hydrogen atoms are omitted for clarity. Color code: sky blue, Zr atom; green, Fe atom; red, O atom; light gray, C atom; pink, O'Pr (isopropanol) group; yellow, OEt (ethanolyl) group.

**Zr<sub>10</sub>Fc<sub>6</sub>** crystallizes in the triclinic space group *P*-1, and each molecule involves a ten-nuclear Zr-oxo core, six Fc ligands, two  $\mu_2$ -OEt and ten terminal coordinated OEt groups (Fig. 1b, c and Fig. S4 online). Similar with **Zr<sub>9</sub>Fc<sub>6</sub>**, the ten-nuclear Zr-oxo core of **Zr<sub>10</sub>Fc<sub>6</sub>** contains a classic octahedral Zr<sub>6</sub>-oxo core, which is further capped by four Zr-oxo units on four different faces to form a tetra-capped octahedron (Fig. S5 online). The Zr ion in the octahedral Zr<sub>6</sub>-oxo core and the capped Zr ion are also coordinated by seven and six O atoms, respectively, and they connected together by  $\mu_4$ -O and  $\mu_2$ -OEt. It is interesting that this ten-nuclear Zr-oxo core also coordinates with six Fc ligands (Fig. S6 online), which is consistent with **Zr<sub>9</sub>Fc<sub>6</sub>**. Besides, the outer coordination space of this ten-nuclear Zr-oxo core contains ten terminal coordinated OEt groups, which indicates that **Zr<sub>10</sub>Fc<sub>6</sub>** also has multiple potential Zr active sites.

To explore whether the nuclearity of the ZrOCs can further increase, we changed the reaction solvent and the metal ion/ligand ratio. Interestingly, a twelve-nuclear ZrOC (**Zr<sub>12</sub>Fc<sub>8</sub>**) that crystallizes in the monoclinic space group *C2/c* was obtained. **Zr<sub>12</sub>Fc<sub>8</sub>** consists of a twelve-nuclear Zr-oxo core, eight Fc ligands, six  $\mu_2$ -O'Pr and eight terminal coordinated O'Pr groups (Fig. S7 online). The twelve-nuclear Zr-oxo core contains two octahedral Zr<sub>6</sub>-oxo core, which shares one edge to form a dumbbell-shaped ten-nuclear Zr-oxo core (Fig. 1a). This ten-nuclear Zr-oxo core is further capped by a Zr-oxo unit on each Zr<sub>6</sub>-oxo octahedron to form the twelve-nuclear Zr-oxo core (Fig. S8 online). The outer coordination space of this Zr-oxo core is surrounded by eight Fc ligands, six  $\mu_2$ -O'Pr and eight terminal coordinated O'Pr groups (Fig. 1b, c and Fig. S9 online). Therefore, compared with **Zr<sub>9</sub>Fc<sub>6</sub>** and **Zr<sub>10</sub>Fc<sub>6</sub>**, **Zr<sub>12</sub>Fc<sub>8</sub>** has higher metal nuclearity and more Fc ligands, but less terminal coordinated solvent molecules, which may render them different catalytic performance.

The experimental powder X-ray diffraction (PXRD) spectra of these three ZrOCs were in agreement with their simulated patterns (Figs. S10–S12 online), indicating their high purity and crystallinity. Thermogravimetric analysis revealed that all three ZrOCs could maintain high structural stability without collapsing before 250 °C (Fig. S13 online). Therefore, these ZrOCs are expected to act as catalysts for the thermocatalytic reaction.

First, we investigated the catalytic performance of these ZrOCs for the hydrogenation of the biomass derivative LA to form  $\gamma$ -valerolactone ( $\gamma$ -GVL), which is an important raw material for the production of aviation fuel and synthetic polymers (Fig. 2a) [39,40]. As Zr-catalysts with strong Lewis acid property are favorable for the substrate adsorption, and the easily tunable activity makes functionalized ligand-modified Zr-based catalysts more attractive [41–43]. Moreover, Fc group has a strong adsorptive activation capacity for hydroxyl radicals, resulting in a kinetic preference for proton-coupled electron transfer hydrogenation [32]. Hence, we think that these Fc-functionalized ZrOCs should have good catalytic activity for this hydrogenation reaction. Using LA as a model substrate, we explored a series of reaction conditions and found the optimum. The results showed that all three ZrOCs can achieve almost 100% conversion of LA at 130 °C within 4 h (Table S5 online). Moreover, the yields of  $\gamma$ -GVL can be up to 89.5%, 91.6% and 95.9% for **Zr<sub>9</sub>Fc<sub>6</sub>**, **Zr<sub>10</sub>Fc<sub>6</sub>** and **Zr<sub>12</sub>Fc<sub>8</sub>** (Fig. 2b), respectively, suggesting they have good catalytic activity and  $\gamma$ -GVL selectivity for this reaction. Interestingly, among three ZrOCs, **Zr<sub>12</sub>Fc<sub>8</sub>** with the largest number of Zr active sites and Fc groups showed the best catalytic performance (Figs. S19–S23 online). To confirm the catalytic activity of these ZrOCs, comparative experiments were conducted without catalysts, and the results showed that the reaction did not proceed. In addition, we also investigated the catalytic activity of the raw materials for the synthesis of **Zr<sub>9</sub>Fc<sub>6</sub>**, **Zr<sub>10</sub>Fc<sub>6</sub>** and **Zr<sub>12</sub>Fc<sub>8</sub>** under the same thermal catalytic conditions (Table S5 online). The results showed that, with ferrocenecarboxylic acid (HFc) ligand as catalyst, the yield of  $\gamma$ -GVL was only 0.5%, while with ZrO<sub>2</sub> as catalyst, the yield of  $\gamma$ -GVL can only achieve 46.7%, confirming the potential of ZrOCs in the thermal catalytic conversion of LA to  $\gamma$ -GVL.

**Fig. 2.** (Color online) Thermalcatalytic conversion of LA to  $\gamma$ -GVL and isopropyl levulinate (IPL). (a) Chemical equation. (b) The yields of  $\gamma$ -GVL and IPL for various catalysts. (c–e) Reaction temperature-, time-, and catalyst dosage-dependent yields of  $\gamma$ -GVL and IPL for **Zr<sub>12</sub>Fc<sub>8</sub>** catalyst. (f) Time-dependent yields of  $\gamma$ -GVL and IPL, and conversion of LA for removing **Zr<sub>12</sub>Fc<sub>8</sub>** catalyst at 0.5 h. (g) Conversion LA to  $\gamma$ -GVL with **Zr<sub>12</sub>Fc<sub>8</sub>** catalyst in five repeating cycles.

Temperature-dependent experiment revealed that the catalytic activity of ZrOCs increased with temperature and reached an optimum value at 130 °C (Fig. 2c). Subsequently, we explored the catalytic effect over time at the optimal temperature conditions. Fig. 2d shows the time function of  $\gamma$ -GVL yield, which can be seen to increase with time and reach an optimum value at 4 h. The amount of catalyst is also a factor affecting the catalytic conversion. As can be seen from Fig. 2e, changing the amount of catalyst had little effect on the LA conversion rate and the  $\gamma$ -GVL yield, suggesting that these ZrOCs can exhibit high activity for LA conversion at low usage levels. We then used methanol, ethanol, *n*-propanol and isopropanol as reaction solvent to investigate the effect of these hydrogen-donating solvents for this reaction (Table S6 online), and the results reveal that isopropanol is the best hydrogen-donating solvent. Finally, to explore the generality of ZrOC catalyst for this transfer hydrogenation of LA-to- $\gamma$ -GVL reaction, we further investigated the catalytic activity of **Zr<sub>12</sub>Fc<sub>8</sub>** for other LA derivatives, including methyl levulinate, ethyl levulinate and propyl levulinate (Table S7 online). The results show that **Zr<sub>12</sub>Fc<sub>8</sub>** has catalytic activity for these LA derivatives, but their conversions are lower than that of LA, and follow the order of methyl levulinate > ethyl levulinate > propyl levulinate, which possibly due to the increased steric hindrance from methyl to propyl.

Because these ZrOCs remain solids after the catalytic reaction, we then demonstrated their heterogeneous nature through several different experiments. First, when the reaction was carried out at 130 °C after 0.5 h, the catalyst was filtered out from the reaction system, and the remaining solution was subjected to reaction at 130 °C for additional 3.5 h. The result shows that there is no further conversion of LA, indicating that this is a heterogeneous catalysis (Fig. 2f). Second, we used inductively-coupled plasma mass spectrometry (ICP-MS) to test the Zr ions of the solid and the reaction solution before and after reaction. The results showed that the Zr content in the solid before and after catalytic reaction was almost unchanged, while for the solution after catalytic reaction, the content of Zr ions was below the detection line, suggesting that these ZrOCs remain solids during the catalytic reaction. In addition, the PXRD (Figs. S28–S30 online) and Fourier transform infrared (FTIR) spectra (Figs. S31–S33 online) of these ZrOCs before and after the catalytic reaction were almost the same, further confirming their stability. As cycle stability is an important parameter for heterogeneous catalyst, we then tested the cycle stability of **Zr<sub>12</sub>Fc<sub>8</sub>**. The result shows that **Zr<sub>12</sub>Fc<sub>8</sub>** could maintain high LA conversions and  $\gamma$ -GVL yields after 5 cycles (Fig. 2g), demonstrating that it has good stability and are heterogeneous catalysts.



Noted that this is the first time to show that ZrOCs can be used as heterogeneous catalysts for LA-to- $\gamma$ -GVL conversion reaction.

Based on the above experimental characterization, the catalytic reaction mechanism should be rationalized as follows: First, Zr acts as a catalytic active site to adsorb the substrate LA, and then LA adsorbs the solvent isopropanol molecule to undergo esterification to form isopropyl levulinate (IL). At this time, Fc group with excellent redox properties adsorbs the isopropanol molecule to assist isopropanol deprotonation and further transfer the proton to IL. Subsequently, intramolecular proton transfer occurs to form 4-hydroxypentanoate (4-HP) (Fig. 3a). Finally, intramolecular dehydration and esterification to form  $\gamma$ -GVL (Fig. 3c). In summary, it is mainly attributed to the variation in the number of active Zr sites and functional Fc groups, which results in different metal-ligand synergistic effects. Moreover, comparative experiments have demonstrated this fact. Specifically, in the catalytic reaction of LA conversion to  $\gamma$ -GVL, individual HFc has almost no catalytic activity, while  $\text{ZrO}_2$  has a yield of 46.7%, and *n*-propanol zirconium ( $\text{Zr}(\text{O}^i\text{Pr})_4$ ) has a yield of 53.5%, indicating that the catalytic site should be on Zr sites. On the other hand, when  $\text{Zr}(\text{O}^i\text{Pr})_4$  and HFc are physically mixed, the  $\gamma$ -GVL yield increases to 67.3% (Table S5 online), which demonstrates the synergistic effect of Zr and HFc. In addition, theoretical calculations are employed to verify the plausibility of this proposed reaction mechanisms. The calculation results show that without Fc, the energy barrier of isopropanol deprotonation reaction is 1.83 eV. However, if HFc ligand is adjacent to Zr, then due to the excellent reactivity of C on Fc group, the isopropanol deprotonation reaction can carry out on Fc group (Fig. S34 online). In this case, the energy barrier of isopropanol deprotonation reaction decreases from 1.83 to 0.535 eV (Fig. 3b) [44]. In brief, the Fc group supplying electrons has a strong adsorption capacity for acetone radicals [33], thus promoting the deprotonation of isopropanol molecules and further transferring the protons to the substrate adsorbed by active Zr site. Under the synergistic effect of metal-ligand cooperative catalysis at a close distance, the hydroesterification reaction is completed, thereby enhancing the conversion efficiency of LA. As a result, almost 100% conversion of LA can be achieved at a lower temperature. Because of such an auxiliary catalytic effect for Fc group, the more and denser it is, the more favorable for the reaction, so **Zr<sub>12</sub>Fc<sub>8</sub>** exhibits the highest catalytic activity.

**Fig. 3.** (Color online) Proposed reaction mechanism and pathways based on density functional theory (DFT) and experimental data for LA-to- $\gamma$ -GVL conversion over the ZrOCs. (a) Molecular structures and their name abbreviation involved in the reaction pathway. (b) Gibbs energy and (c) reaction pathways for LA-to- $\gamma$ -GVL conversion over the ZrOCs.

Since the functional Fc group can modulate the redox properties of ZrOCs, we further used them as catalysts to investigate the thermally excited oxidation reaction. Functionalized hydroquinone are valuable intermediates in the synthesis of drugs and fine chemicals and play an important role in biological systems [45–47]. However, conventional catalysts are mostly homogeneous systems, which have problems such as difficulty in separating the products and recovering the catalyst, and corrosion of the reactor. These Fc-functionalized ZrOCs with superior redox properties and good solvent stability are expected to be heterogeneous catalysts to accomplish the above reactions, and to solve the problems of metal leaching and low product selectivity. Therefore, we investigated the catalytic performance of these three ZrOCs by using TMP as model substrate, acetonitrile as solvent and hydrogen peroxide as oxidant (Fig. 4a).

**Fig. 4.** (Color online) Thermalcatalytic conversion of TMP to TMBQ. (a) Chemical equation. (b) The conversion rate of TMP and yield of TMBQ for various catalysts. (c) The TMBQ yield for **Zr<sub>12</sub>Fc<sub>8</sub>** catalyst after the addition of different radical scavengers. (d) EPR spectra of **Zr<sub>12</sub>Fc<sub>8</sub>** in  $\text{CH}_3\text{CN}$  with TMP and  $\text{H}_2\text{O}_2$  at 80 °C. (e) Catalyst and (f)  $\text{H}_2\text{O}_2$  dosage dependent conversion and yield for the oxidation of TMP to TMBQ. (g) Yield of TMBQ with **Zr<sub>12</sub>Fc<sub>8</sub>** catalyst in five repeating cycles.

At 80 °C, all three ZrOCs exhibited excellent catalytic activity for the conversion of TMP to TMBQ. Among them, **Zr<sub>12</sub>Fc<sub>8</sub>** coordinated with more Fc ligands exhibited the best performance, achieving 99.3% TMP conversion efficiency and 98.8% TMBQ yield within 30 min (Figs. S24–S27 online), which are higher than that of **Zr<sub>9</sub>Fc<sub>6</sub>** (94.9% TMP conversion rate and 87.0% TMBQ yield) and **Zr<sub>10</sub>Fc<sub>6</sub>** (96.0% TMP conversion rate and 91.0% TMBQ yield) (Fig. 4b). This difference is mainly attributed to **Zr<sub>12</sub>Fc<sub>8</sub>** having more catalytically active Zr sites and auxiliary catalytic Fc groups. In addition, to study the catalytic activity of ZrOCs, a series of control experiments were conducted. Without the addition of catalysts and oxidants, TMP was difficult to convert to TMBQ (Table S8 online). According to the reported works, there are two main pathways for oxidizing TMP to TMBQ [48]. Therefore, we selected different radical scavengers to study the possible pathways reflected by ZrOCs in the catalytic oxidation process. As can be seen in Fig. 4c, when oxygen radical scavenger Ph<sub>2</sub>NH and carbon radical scavenger 2,2,6,6-tetramethylpiperidin-1-yl)oxyl (TEMPO) were added, there was almost no effect on the overall catalytic effect. However, when methanol was added as hydroxyl radical scavenger, the yield of TMBQ decreased significantly. Therefore, we determined that these ZrOCs produced hydroxyl radicals during the catalytic oxidation of TMP. Further, we confirmed the existence of hydroxyl radicals through the electron paramagnetic resonance (EPR) test (Figs. S14–S17 online).

In addition, the effects of different oxidants were investigated. The use of oxygen does not promote the reaction, while the use of tert-butyl hydroperoxide as an oxidizing agent can promote the reaction, but with poor product yield (Table S9 online). The amount of oxidant used is a factor affecting the catalytic performance. Experimental results showed that without the addition of oxidant, almost no TMBQ can be detected. As the amount of oxidant increased, the yield of TMBQ increased accordingly (Fig. 4f). Reaction temperature is an important factor driven by thermodynamics. As the temperature increased, the yield of TMBQ increased accordingly and reached its highest yield at 80 °C (Table S10 online). At the same time, we explored the function of catalytic performance over time. As shown in the Table S11 (online), the catalytic effect was optimal at 30 min. A 90.4% TMBQ yield can also be achieved by reacting at 60 °C for 30 min, demonstrating the excellent catalytic activity of these ZrOCs. Considering that the amount of catalyst used would also affect the catalytic effect, as expected, as the amount of catalyst increased, the yield increased accordingly and reached its highest yield at 30 mg (Fig. 4e). We then used methanol, ethanol, n-propanol, N,N-dimethylformamide, petroleum ether, dichloromethane, 1,4-dioxane and n-hexane as reaction solvent to investigate the effect of these solvent for this reaction (Table S13 online), and the results reveal that acetonitrile is the best reaction solvent. The advantage of heterogeneous catalysts is that they can be recycled. Therefore, we first explored the heterogeneity of these three ZrOCs in the catalytic process. The filtrate after the reaction was tested by ICP, and the results showed that the metal content was particularly low and did not reach the integration limit (Table S14 online). Therefore, no active metal components were dissolved in the solvent to play a catalytic role. The cyclic tests were also performed by using the recovered catalysts. The results showed that after five rounds of catalysis, the yield of **Zr<sub>12</sub>Fc<sub>8</sub>** basically did not change (Fig. 4g), demonstrating the excellent performance and stability of these ZrOCs in catalyzing phenol oxidation. The powder after the reaction was tested by FTIR, and the peak shape retained their characteristic groups, further confirming the stability of these catalysts. In addition, the catalytic activity of **Zr<sub>12</sub>Fc<sub>8</sub>** for other phenol derivatives, including 2,6-dimethylphenol, 3,5-dimethoxyphenol, 2,5-dimethylphenol and 2,6-di-tert-butylphenol, was also investigated. The results show that these phenol derivatives can also be effectively converted into corresponding p-benzoquinone with medium yield (Table S12 online).

To investigate the catalytic mechanism, we used DFT calculation to compare the reaction energy barriers when Zr, Zr–O–O and Fc group were used as catalytic active sites (Fig. 5c and Fig. S35 online). The results revealed that the rate-determining step (rds) of Fc group site is the first step (the catalyst adsorbs phenol and becomes phenoxide ion), with reaction energy of –0.536 eV, while the rds of Zr site is the second step (the phenoxide ion reacts with ·O<sub>2</sub>H to produce 2,5-cyclohexadienone-1-one, 4-hydroperoxide), with reaction energy of 0.118 eV (Fig. 5a–c). Thus, Zr site itself has poor activity. However, if Zr–O–O is formed by H<sub>2</sub>O<sub>2</sub>, then the rds becomes the first step, with reaction energy of –1.52 eV (Fig. 5b, c). Thus, Zr site has better activity than Fc group. Fc group plays the role of Fenton reagent, which can produce hydroxyl radical (·OH) and superoxide radical (·O<sub>2</sub>H), but its own ability to catalyze phenol oxidation is not as good as Zr–O–O, indicating that it plays an auxiliary catalytic role. This explains why HFc ligand itself has activity in experiments, but is not as good as ZrOCs. It also corresponds to the ·OH and ·O<sub>2</sub>H signals detected by EPR experiments (Figs. S14–S17 online). At the same time, it shows that although Zr is active site, it must be oxidized by H<sub>2</sub>O<sub>2</sub> into Zr–O–O to produce activity, which also corresponds to the Zr–O–O (Fig. 4d and Fig. S18 online) signal found by EPR experiments [49]. However, with only Zr as the active site, the reaction cannot proceed efficiently and must be assisted by Fc group, the synergistic effect of the metal and the ligand improves the efficiency of the reaction. This conclusion was also confirmed

experimentally, where the TMBQ yield is only 30.1% for  $\text{ZrO}_2$  alone, 47.6% for  $\text{Zr}(\text{O}^i\text{Pr})_4$ , and 20.0% for HFc ligand alone, while the Fc-modified  $\text{Zr}_{12}\text{Fc}_8$  can reach 98.8% TMBQ yield (Table S8 online), further indicating that the synergistic effect of the metal-ligand promoted the efficient reaction. On the other hand, the difference properties for the three ZrOCs were also mainly attributed to the number of active and auxiliary sites, for which the catalytic activity was enhanced with the increase in the number of Zr and Fc group, and thus  $\text{Zr}_{12}\text{Fc}_8$  exhibited the best performance. Totally, theoretical calculations show that Zr as the active sites first react with  $\text{H}_2\text{O}_2$  to generate  $\text{Zr-O-O}$ , while Fc group as Fenton reagent activates  $\text{H}_2\text{O}_2$  to generate oxygen radicals ( $\cdot\text{OH}$  and  $\cdot\text{O}_2\text{H}$ ) required for the reaction (Fig. 5b). And then  $\text{Zr-O-O}$  adsorbs the substrate TMP, and  $\cdot\text{OH}$  activates TMP to generate phenoxy radicals, which is further activated by  $\cdot\text{O}_2\text{H}$  to generate peroxyquinone intermediate, and finally deletes a molecule of water to generate TMBQ (Fig. 5d). This result shows that the Fenton effect of Fc group combined with the synergistic effect of metal-ligand is used to efficiently catalyze the oxidation of phenol and its derivatives.

**Fig. 5.** (Color online) Proposed reaction mechanism and pathways based on DFT and experimental data for TMP-to-TMBQ conversion over the ZrOCs. (a) Molecular structures and their name abbreviation involved in the reaction pathway. (b) Reaction pathways and intermediate architectures, (c) corresponding Gibbs energy, and (d) reaction mechanism for TMP-to-TMBQ conversion over the ZrOCs with  $\text{H}_2\text{O}_2$  as oxidant.



#### 4. Conclusion

In summary, we first report three ZrOCs constructed from functionalized Fc groups that exhibit incremental nucleation by ligand modulation engineering. Notably, the modification of Fc groups with excellent redox properties confers high catalytic activity of these ZrOCs for oxidation and reduction reactions. Therefore, these ZrOCs were further explored as heterogeneous catalysts in thermocatalytic levulinic acid hydrogenation reactions and phenol oxidation reactions. The corresponding experimental evidences and theoretical calculations showed that the intramolecular metal-ligand synergy plays a key role in the whole catalytic process, and Fc group has a strong electron-donating ability and acts as a hydrogen transfer reagent and Fenton reagent in the reaction to complete the catalysis efficiently in concert with the active Zr sites; moreover, the catalytic activity is higher as the number of active Zr sites and Fc groups increases, so that **Zr<sub>12</sub>Fc<sub>8</sub>** exhibited the highest catalytic performance. This study demonstrates an effective strategy to modulate the catalytic performance of ZrOCs using ligand engineering, which may broaden the application of ZrOCs in the field of catalysis.

#### Conflict of interest

The authors declare that they have no conflict of interest.

#### Acknowledgments

This work was supported by the National Key R&D Program of China (2023YFA1507204), the National Natural Science Foundation of China (22271104, 22225109, 22071109, and 22201046), the Excellent Youth Foundation of Jiangsu Natural Science Foundation (BK20211593), Young Top Talents of Pearl River Talent Program of Guangdong Province (2021QN02L617), Guangdong Basic and Applied Basic Research Foundation (2023A1515030097), and the Open Fund of Energy and Materials Chemistry Joint Laboratory of South China Normal University and Guangzhou Tinci Materials Technology (SCNU-TINCI-202204).

#### Author contributions

Su-Juan Yao, Jiang Liu, and Ya-Qian Lan conceived and designed the idea. Su-Juan Yao and Ying-Lin Li synthesized the compounds. Su-Juan Yao and Long-Zhang Dong designed and conducted characterizations. Su-Juan Yao, Ning Li, Jiao-Min Lin, Jiang Liu, and Ya-Qian Lan discussed the result and prepared the manuscript. All the authors reviewed and contributed to this paper.

## Appendix A. Supplementary materials

Supplementary materials to this article can be found online at

## References

- [1] Zhang Y, Zhao Y, Otroshchenko T, et al. Control of coordinatively unsaturated Zr sites in  $\text{ZrO}_2$  for efficient C–H bond activation. *Nat Commun* 2018; 9: 3794.
- [2] Cheng K, Zhou W, Kang JC, et al. Bifunctional catalysts for one-step conversion of syngas into aromatics with excellent selectivity and stability. *Chem* 2017; 3: 334–347.
- [3] Kattel S, Yan BH, Yang YX, et al. Optimizing binding energies of key intermediates for  $\text{CO}_2$  hydrogenation to methanol over oxide-supported copper. *J Am Chem Soc* 2016; 138: 12440–12450.
- [4] Yang M, Yu JF, Zimina A, et al. Probing the nature of zinc in copper-zinc-zirconium catalysts by operando spectroscopies for  $\text{CO}_2$  hydrogenation to methanol. *Angew Chem Int Edit* 2023; 135: e202216803.
- [5] Pereira GKR, Guilardi LF, Dapieve KS, et al. Experimental and theoretical determination of the electronic structure and optical properties of three phases of  $\text{ZrO}_2$ . *Phys Rev B Condens Matter* 2018; 85: 57–65.
- [6] Tang B, Dai WL, Sun XM, et al. Mesoporous Zr-beta zeolites prepared by a post-synthetic strategy as a robust lewis acid catalyst for the ring-opening aminolysis of epoxides. *Green Chem* 2015; 17: 1744–1755.
- [7] Bregante DT, Flaherty DW. Periodic trends in olefin epoxidation over group IV and V framework-substituted zeolite catalysts: A kinetic and spectroscopic study. *J Am Chem Soc* 2017; 139: 6888–6898.
- [8] Bezrukov AA, Törnroos KW, Le Roux E, et al. Incorporation of an intact dimeric  $\text{Zr}_{12}$  oxo cluster from a molecular precursor in a new zirconium metal-organic framework. *Chem Commun* 2018; 54: 2735–2738.
- [9] Yuan S, Qin J-S, Su J, et al. Sequential transformation of zirconium(IV)-MOFs into heterobimetallic MOFs bearing magnetic anisotropic cobalt(II) centers. *Angew Chem Int Edit* 2018; 57: 12578–12583.
- [10] Feng D, Chung W-C, Wei Z, et al. Construction of ultrastable porphyrin Zr metal-organic frameworks through linker elimination. *J Am Chem Soc* 2013; 135: 17105–17110.

- [11] Feng D, Gu Z-Y, Li J-R, et al. Zirconium-metalloporphyrin PCN-222: Mesoporous metal-organic frameworks with ultrahigh stability as biomimetic catalysts. *Angew Chem Int Edit* 2012; 51: 10307–10310.
- [12] Mondloch JE, Bury W, Fairen-Jimenez D, et al. Vapor-phase metalation by atomic layer deposition in a metal-organic framework. *J Am Chem Soc* 2013; 135: 10294–10297.
- [13] Furukawa H, Gandara F, Zhang YB, et al. Water adsorption in porous metal-organic frameworks and related materials. *J Am Chem Soc* 2014; 136: 4369–4381.
- [14] Zhao Y, Qi S, Niu Z, et al. Robust corrole-based metal-organic frameworks with rare 9-connected Zr/Hf-oxo clusters. *J Am Chem Soc* 2019; 141: 14443–14450.
- [15] Wang L, Jin P, Duan S, et al. *In-situ* incorporation of copper(II) porphyrin functionalized zirconium MOF and TiO<sub>2</sub> for efficient photocatalytic CO<sub>2</sub> reduction. *Sci Bull* 2019; 64: 926-933.
- [16] Zhang Y, Kokculer IY, de Azambuja F, et al. Dynamic environment at the Zr<sub>6</sub> oxo cluster surface is key for the catalytic formation of amide bonds. *Catal Sci Technol* 2023; 13: 100–110.
- [17] Sui J, Gao M-L, Qian B, et al. Bioinspired microenvironment modulation of metal-organic framework-based catalysts for selective methane oxidation. *Sci Bull* 2023; 68: 1886-1893.
- [18] Li X-M, Wang Y, Mu Y, et al. Oriented construction of efficient intrinsic proton transport pathways in MOF-808. *J Mater Chem A*, 2022; 10: 18592–18597.
- [19] Guo B, Cheng X, Tang Y, et al. Dehydrated UiO-66(SH)<sub>2</sub>: The Zr-O cluster and its photocatalytic role mimicking the biological nitrogen fixation. *Angew Chem Int Edit* 2022; 61: e202117244.
- [20] An B, Li Z, Song Y, et al. Cooperative copper centres in a metal-organic framework for selective conversion of CO<sub>2</sub> to ethanol. *Nat Catal* 2019; 2: 709–717.
- [21] Zhang Y, de Azambuja F, Parac-Vogt TN. The forgotten chemistry of group(IV) metals: A survey on the synthesis, structure, and properties of discrete Zr(IV), Hf(IV), and Ti(IV) oxo clusters. *Coord Chem Rev* 2021; 438: 213886.
- [22] Van den Eynden D, Pokratath R, De Roo J. Nonaqueous chemistry of group 4 oxo clusters and colloidal metal oxide nanocrystals. *Chem Rev* 2022; 122: 10538–10572.
- [23] Xie W-L, Li X-M, Lin J-M, et al. Keeping superprotonic conductivity over a wide temperature region via sulfate hopping sites-decorated zirconium-oxo clusters. *Small* 2022; 18: 2205444.

- [24] Sun S-N, Niu Q, Lin J-M, et al. Sulfur atom-directed metal–ligand synergistic catalysis in zirconium/hafnium-oxo clusters for highly efficient amine oxidation. *Science Bulletin*; 2024, 69: 492-501.
- [25] Rimoldi M, Howarth AJ, DeStefano MR, et al. Catalytic zirconium/hafnium-based metal-organic frameworks. *ACS Catal* 2017; 7: 997–1014.
- [26] Peng Q, Jiang Y, Xu B–B, et al. Zr oxo cluster for cascade conversion of furfural to alkyl levulinates. *ChemCatChem* 2023; 15: e202201352.
- [27] Xu M, Li D, Sun K, et al. Interfacial microenvironment modulation boosting electron transfer between metal nanoparticles and MOFs for enhanced photocatalysis. *Angew Chem Int Edit* 2021; 60 : 16372–16376.
- [28] Zhang H, Si S, Zhai G, et al. The long-distance charge transfer process in ferrocene-based mofs with FeO<sub>6</sub> clusters boosts photocatalytic CO<sub>2</sub> chemical fixation. *Appl Catal B* 2023; 337: 122909.
- [29] Xu J, Tan J, Song C, et al. Self-immolative amphiphilic poly(ferrocenes) for synergistic amplification of oxidative stress in tumor therapy. *Angew Chem Int Edit* 2023; e202303829.
- [30] Liu J-J, Li N, Sun J-W, et al. Ferrocene-functionalized polyoxo-titanium cluster for CO<sub>2</sub> photoreduction. *ACS Catal* 2021; 11: 4510–4519.
- [31] Liu J-J, Sun S-N, Liu J, et al. Achieving high-efficient photoelectrocatalytic degradation of 4-chlorophenol via functional reformation of titanium-oxo clusters. *J Am Chem Soc* 2023; 145: 6112–6122.
- [32] Li M, Sun H, Yang J, et al. Mono-coordinated metallocene ligands endow metal-organic frameworks with highly efficient oxygen evolution and urea electrolysis. *Chem Eng J* 2022; 430: 132733.
- [33] Li Q, Wang Z–M, Chen Y, et al. CO<sub>2</sub>-to-CH<sub>4</sub> electroreduction over scalable Cu-porphyrin based organic polymers promoted by direct auxiliary bonding interaction. *J Mater Chem A* 2022; 10: 25356–25362.
- [34] Valekar AH, Cho K–H, Chitale SK, et al. Catalytic transfer hydrogenation of ethyl levulinate to  $\gamma$ -valerolactone over zirconium-based metal-organic frameworks. *Green Chem* 2016; 18: 4542–4552.
- [35] Dutta S, Yu IKM, Tsang DCW, et al. Green synthesis of gamma-valerolactone (GVL) through hydrogenation of biomass-derived levulinic acid using non-noble metal catalysts: A critical review. *Chem Eng J* 2019; 372: 992–1006.
- [36] Li Y, Qin Y, Shang Y, et al. Mechano-responsive leapfrog micelles enable interactive apoptotic and ferroptotic cancer therapy. *Adv Funct Mater* 2022; 32: 2112000.

- [37] Lin J, Yang H, Zhang Y, et al. Ferrocene-based polymeric nanoparticles carrying doxorubicin for oncotherapeutic combination of chemotherapy and ferroptosis. *Small* 2023; 19: 2205024.
- [38] Zhang L, Fan X, Yi X, Lin X, Zhang J. Coordination-delayed-hydrolysis method for the synthesis and structural modulation of titanium-oxo clusters. *Acc Chem Res* 2022; 55: 3150–3161.
- [39] Huang X, Liu K, Vrijburg WL, et al. Hydrogenation of levulinic acid to  $\gamma$ -valerolactone over Fe-Re/TiO<sub>2</sub> catalysts. *Appl Catal B* 2020; 278: 119314.
- [40] Li Z, Hao H, Lu J, et al. Role of the Cu-ZrO<sub>2</sub> interface in the hydrogenation of levulinic acid to  $\gamma$ -valerolactone. *J Energy Chem* 2021; 61: 446–458.
- [41] Wan F, Yang B, Zhu J, et al. The transfer hydrogenation of high concentration levulinic acid to  $\gamma$ -valerolactone catalyzed by glucose phosphate carbamide zirconium. *Green Chem* 2021; 23: 3428–3438.
- [42] Song J, Hua M, Huang X, et al. Highly efficient Meerwein-Ponndorf-Verley reductions over a robust zirconium-organoboronic acid hybrid. *Green Chem* 2021; 23: 1259–1265.
- [43] Song J, Zhou B, Zhou H, et al. Porous zirconium-phytic acid hybrid: A highly efficient catalyst for Meerwein-Ponndorf-Verley reductions. *Angew Chem Int Edit* 2015; 54: 9399–9403.
- [44] Liang J, Gao X, Guo B, et al. Ferrocene-based metal-organic framework nanosheets as a robust oxygen evolution catalyst. *Angew Chem Int Edit* 2021; 60: 12770–12774.
- [45] Evtushok VY, Suboch AN, Podyacheva OY, et al. Highly efficient catalysts based on divanadium-substituted polyoxometalate and n-doped carbon nanotubes for selective oxidation of alkylphenols. *ACS Catal* 2018; 8: 1297–1307.
- [46] Chang S, Chen Y, An H, et al. Polyoxometalate-based supramolecular porous frameworks with dual-active centers towards highly efficient synthesis of functionalized p-benzoquinones. *Green Chem* 2021; 23: 8591–8603.
- [47] Chang S, Chen Y, An H, et al. Highly efficient synthesis of p-benzoquinones catalyzed by robust two-dimensional pom-based coordination polymers. *ACS Appl Mater Interfaces* 2021; 13: 21261–21271.
- [48] Kholdeeva OA, Zalomaeva OV. Recent advances in transition-metal-catalyzed selective oxidation of substituted phenols and methoxyarenes with environmentally benign oxidants. *Coord Chem Rev* 2016; 306: 302–330.
- [49] Ji P, Feng X, Veroneau SS, et al. Trivalent zirconium and hafnium metal-organic frameworks for catalytic 1,4-dearomative additions of pyridines and quinolines. *J Am Chem Soc* 2017; 139: 15600–15603.

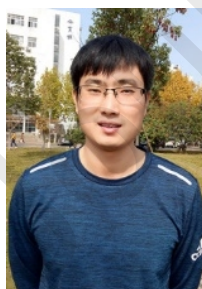




Su-Yuan Yao received her Bachelor's and M.S. degrees from Nanjing Normal University (2022). Now, she is a Ph.D. candidate at South China Normal University. Her current research focuses on the synthesis of crystalline compounds as catalysts for catalyzing organic reactions.



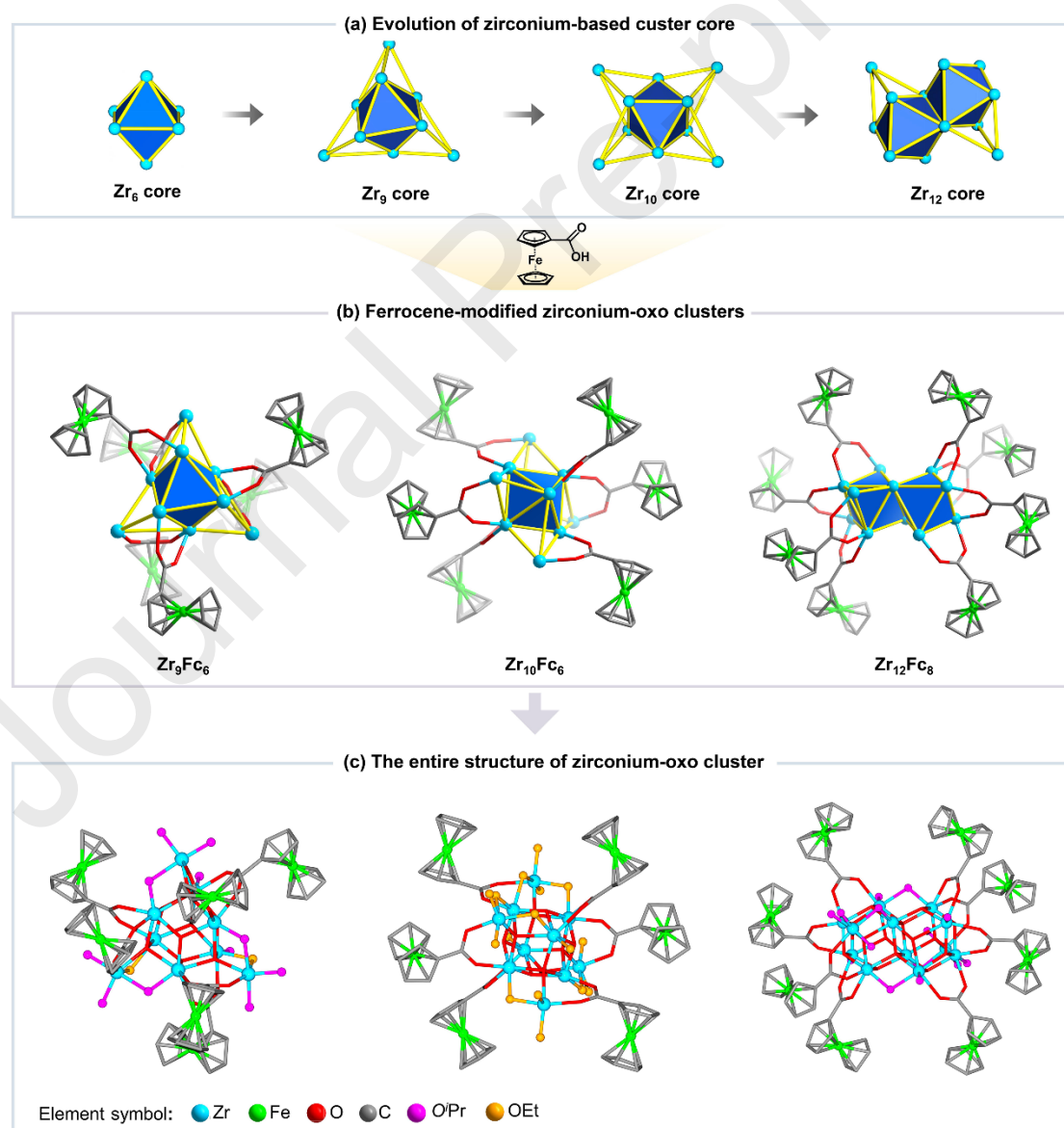
Jiao-Min Lin received his B.S. and M. S. degrees from Guangzhou University under the supervision of Prof. Wen Dong. He subsequently obtained his Ph.D. degree from Sun Yat-sen University under the direction of Prof. Jie-Peng Zhang. After that, he worked as a teacher at College of Chemistry and Materials Science, Shanghai Normal University. In 2021, he joined Prof. Ya-Qian Lan's group at School of Chemistry, South China Normal University. His current research interest focuses on the syntheses, structures and properties of metal-organic framework (MOF) and polyoxometalates (POMs).

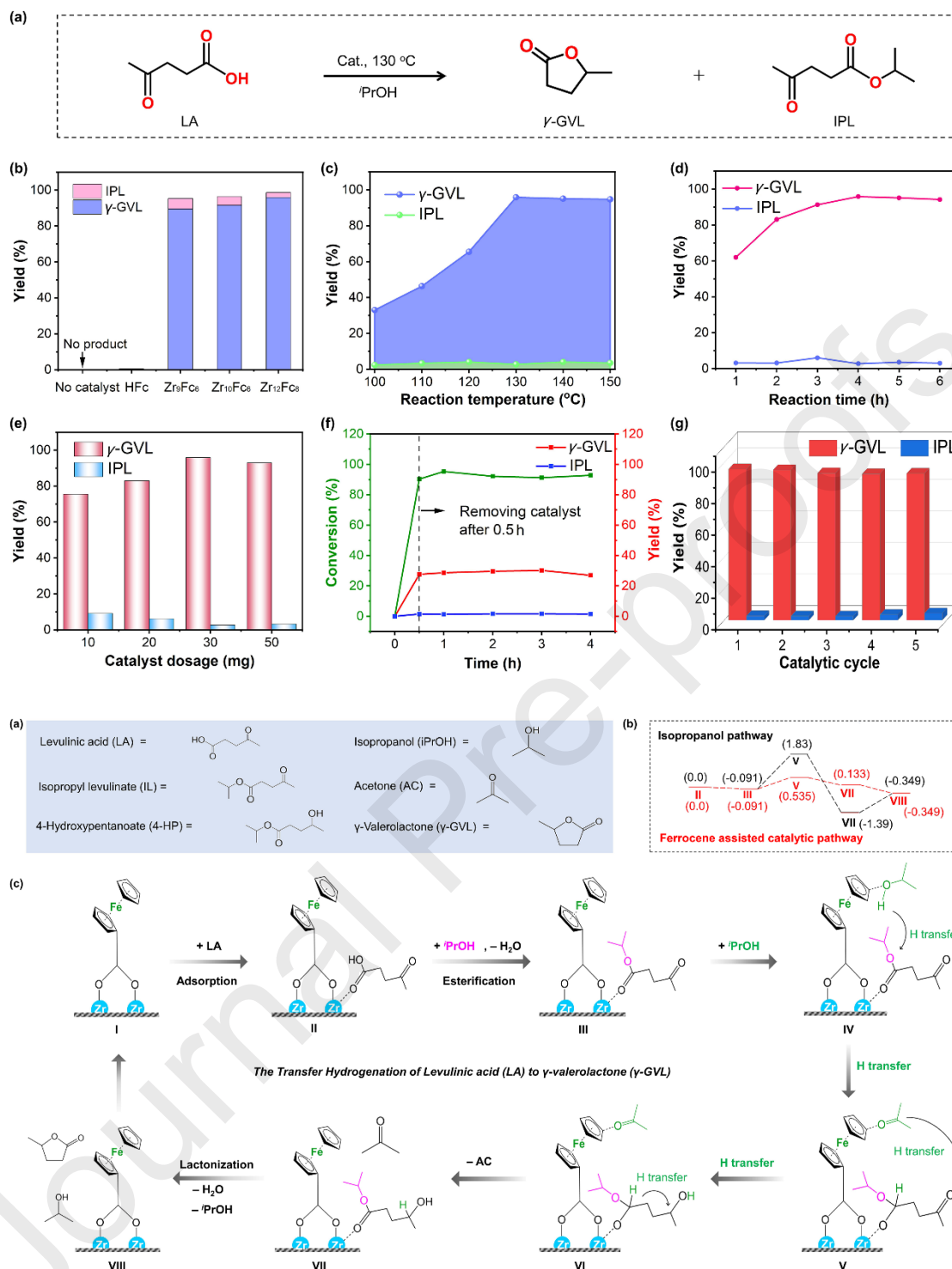


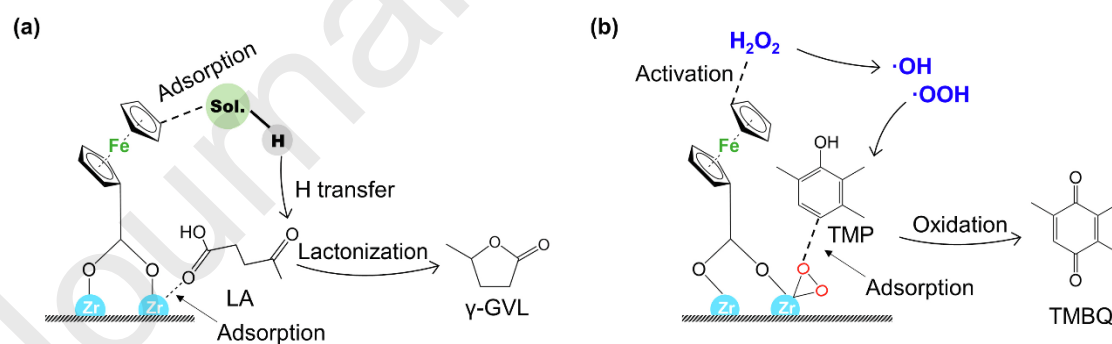
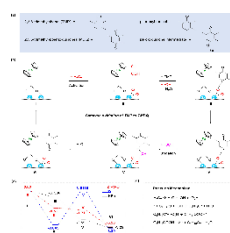
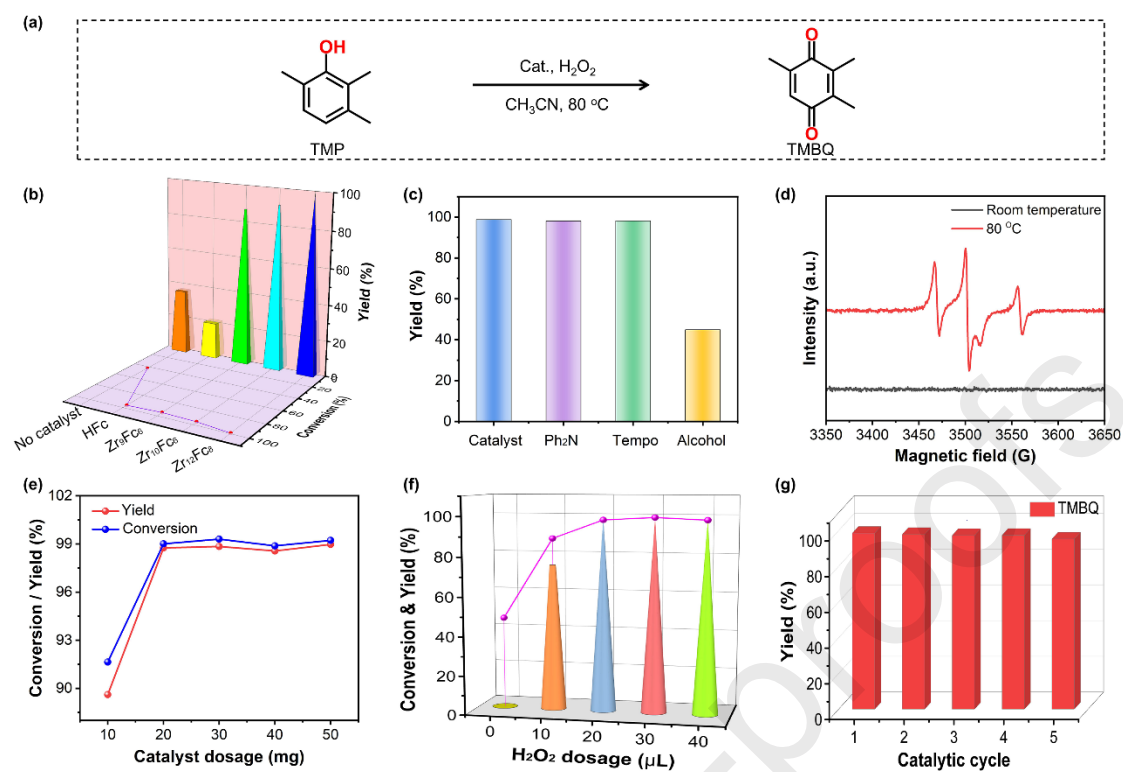
Jiang Liu joined Prof. Ya-Qian Lan's group at College of Chemistry and Materials Science, Nanjing Normal University in 2016. In 2022, he joined South China Normal University and became a professor of Chemistry. His research interest focuses on the development of molecular-based metal cluster and metal-organic crystalline materials applied in energy storage and conversion, proton conductivity and photo/electric heterogeneous catalysis.



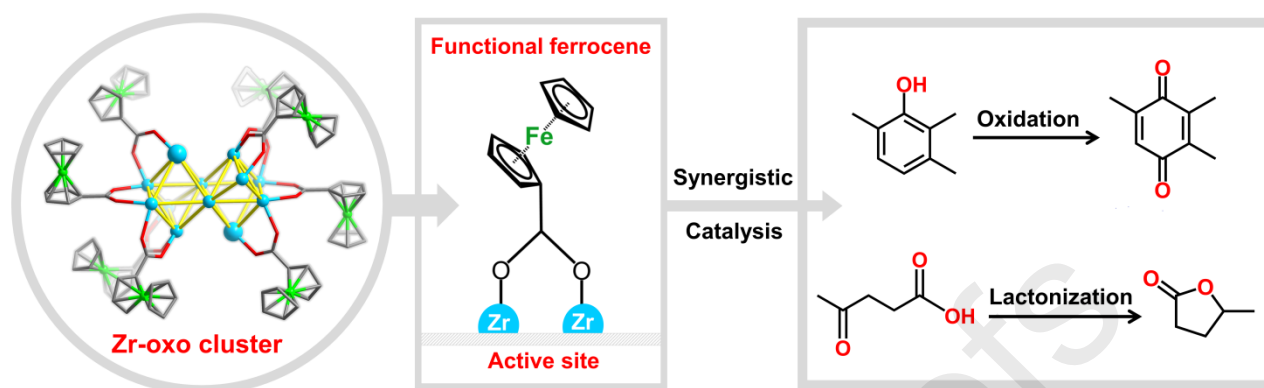
Ya-Qian Lan received his B.S. and Ph.D. degrees (2009) from Northeast Normal University, under the supervision of Prof. Zhong-Min Su. In 2010, he joined the National Institute of Advanced Industrial Science and Technology (AIST, Japan) working as a JSPS postdoctoral fellow. In 2012, he became a professor of Chemistry at Nanjing Normal University. He joined South China Normal University in 2021. His current research interest focuses on the synthesis of new crystalline materials and catalytic research related to clean energy applications.







## High-performance thermocatalytic redox reactions



Three ferrocene-functionalized Zr-oxo clusters featuring increased nuclearity and regular structural variation were synthesized and treated as outstanding catalysts to achieve high-performance thermocatalytic redox reactions, in which LA-to- $\gamma$ -valerolactone and phenol-to-quinone conversions can be finished at lower temperature and in shorter time, under the synergistic catalysis of active Zr site and functional ferrocene group. (Color online)